ELECTRONIC STRUCTURE AND MÖSSBAUER HYPERFINE INTERACTIONS OF Au(I) COMPOUNDS

Diana Guenzburger

Centro Brasileiro de Pesquisas Físicas
Avenida Wenceslau Braz 71
Rio de Janeiro, RJ-22.290, Brasil

and

D. E. Ellis*

Department of Chemistry and Physics
Northwestern University, Evanston, IL 60201, U.S.A.

ABSTRACT

The electronic structure of the linear Au(I) complexes $[AuX_2]^{-1}$, where X=CN, Cl, and F has been studied in the self-consistent one-electron statistical exchange model. The relative importance of gold 5d, 6s, and 6p states in chemical bonding and for hyperfine interactions is examined, using an LCAO decomposition of the molecular eigenstates. The variation of the isomer shift and quadrupole splitting of ^{197}Au with covalency is studied theoretically. The effect of pressure on these hyperfine interactions for $K[Au(CN)_2]$ is investigated by considering different interatomic distances. In this latter case, the main discrepancies with respect to experiment found are believed to arise from bonding with exterior atoms. Relativistic effects are briefly explored by comparison of Dirac-Slater relativistic and non-relativistic results for the cyanide anion.

---

* Research supported in part by the National Science Foundation, Grant DMR 77-22646.

I INTRODUCTION

The element Au in oxidation state +1 is known to form a large number of compounds in linear coordination; the properties of these complexes vary according to the nature of the ligands. The measurement of hyperfine interactions obtained from Mössbauer spectroscopy can give valuable information about these compounds; however, only a quantitative calculation of the electronic structure of the Au(I) compounds or complex ions can give insight into the nature of the Au-ligand bond and provide the means to interpret and calculate the hyperfine interactions.

The study of linear Au(I) compounds by Mössbauer spectroscopy of ^{197}Au has resulted in some interesting features[1-4]. A negative sign of the electric field gradient (EFG) was found for $KAu(CN)_2$[2]. By means of a simple atomic model, this may be considered as evidence of the dominant role of the $6p_z$ electrons in producing the quadrupole splitting[1,5], since p_z electrons give a negative contribution. In contrast, the electric field gradient of the covalent compounds of the lighter Mössbauer isotope ^{57}Fe has been interpreted as arising from distortions in the partially filled 3d shell.

Another aspect of the Mössbauer parameters of Au(I) compounds is the strikingly linear relation found between the isomer shifts (δ) and the quadrupole splittings (Δ) for the large number of compounds measured[3,4,6]; both δ and $|\Delta|$ increase with increasing covalency of the Au-ligand bond. Although this last feature also seems to point out the importance of the outer 6s and 6p electrons, the role of the 5d eletrons has been the subject of controversy. Some authors consider it to be negligible[3,4], while others[2,7,8] suggest that bonding through the 5d orbital has an important effect by depletion of this orbital through the mechanism known as back-donation to ligand π orbitals. This last view is supported by the variation with pressure observed for the isomer shift and quadrupole splitting of $KAu(CN)_2$[9].

The theoretical interpretation of electronic effects in the quadrupole splittings of transition metal compounds has so far largely relied on atomic models. Covalency effects are taken into account by considering only the population of the outer d, s and p orbitals, together with atomic values of $\langle r^{-3} \rangle$. Models based on the orthogonalization of atomic core orbitals and valence ligand orbitals (overlap distortion) have also been derived to explain measured EFG values in iron compounds[10]. Polarization of the inner shells is approximately taken into account by inclusion of the Sternheimer[11a] factor. In the case of Au(I) compounds, semi-empirical molecular orbital (MO) calculations[12] were performed for the valence electrons, in order to interpret the Mössbauer hyperfine interactions; however, only atomic populations were obtained by this technique.

We have performed self-consistent MO calculations using the one-electron Hartree-Fock-Slater theory and the Discrete Variational method[13] for three Au(I) linear complex ions exhibiting different degrees of covalency, namely $[Au(CN)_2]^{-1}$, $AuCl_2^{-1}$ and AuF_2^{-1}. All electrons were included in the calculations. The results obtained were used to calculate the electronic density at the nucleous $\rho(0)$, which is related to the isomer shift by:

$$\delta = \frac{2}{3} e^2 \pi Z S'_z \left[\langle r^2 \rangle_E - \langle r^2 \rangle_G\right]\left[\rho_A(0) - \rho_S(0)\right] \equiv A\Delta\rho(0) \qquad (1)$$

where

$$\left[\langle r^2 \rangle_E - \langle r^2 \rangle_G\right]$$

is the difference between the mean square radius of the nucleus in the excited and ground states in the Mössbauer transition, and $\rho_A(0)$ and $\rho_S(0)$ refer to charge density at absorber and source nuclei. $\rho(0)$ is taken as

$$\rho(0) = \sum_i n_i \, |\Psi_i(0)|^2 \qquad (2)$$

where n_i is the occupation of the one-electron molecular wave function ψ_i, and S'_z is a correction factor for relativistic effects[14]. The electronic contribution to the quadrupole splitting of the I=3/2 ground state of the 77.3 KeV transition of ^{197}Au for linear complexes is given by

$$\Delta = \frac{1}{2} e^2 Qq \qquad (3)$$

where Q is the quadrupole moment of the nucleus and q is the matrix element

$$q = - \sum_i n_i \langle \psi_i \left| \frac{3\cos^2\theta - 1}{r^3} \right| \psi_i \rangle \qquad (4)$$

calculated over the molecular orbitals ψ_i. In Mössbauer spectroscopy, the quadrupole splitting is measured by moving the absorber relative to the source, and so changing the energy of the nuclear transition by the Doppler effect. For this reason it is customary to report values of Δ in units of velocity; for the 77.3 keV transition of ^{197}Au, we have 1 mm/sec=41.31x10^{-20} ergs.

This manner of obtaining Δ is now consistent with the molecular orbital picture of the complexes, in which covalency and overlap effects are taken into account simultaneously. The use of the Sternheimer factor may be eliminated by inclusion of all core electrons in the SCF procedure.

II DETAILS OF THE CALCULATIONS

II.a The Discrete Variational Method (DVM)

The DVM method has been described in detail elsewhere[13]. If one defines an error function for approximate solution of the Schrödinger equation

$$f_i(\vec{r}) = (H-E_i)\psi_i(\vec{r}) \tag{5}$$

where ψ_i are one-electron molecular wave functions expanded on a basis of symmetrized atomic orbitals χ_j,

$$\psi_i(\vec{r}) = \sum_j \chi_j(\vec{r})\ C_{ji} \quad , \tag{6}$$

the coefficients $\underset{\approx}{C}$ may be determined by minimizing a weighted average of $f_i(\vec{r})$ over a discrete set of sample points.

One then obtains a secular equation

$$(\underset{\approx}{H} - \underset{\approx\approx}{ES})\underset{\approx}{C} = 0 \tag{7}$$

where the matrix elements are simply sums over sample points. The Hamiltonian is given by

$$h = -\frac{1}{2}\nabla^2 + V_{coulomb} + V_x \tag{8}$$

where the local exchange potential V_x is (in Hartree a.u.)

$$V_x(\vec{r}) = -3\alpha\left[(3/8\pi)\rho(\vec{r})\right]^{1/3} \tag{9}$$

The atomic functions are taken to be numerical self-consistent Hartree-Fock-Slater orbitals in the $X\alpha$ approximation[15], calculated with the same value of α. Here the parameter α is given the value 2/3 [16].

The self-consistency of the molecular calculations is obtained by converging the atomic orbital populations, which are used to generate the molecular potential. We use a variant of the "standard" Mulliken[17] populations, in which the overlap population is partitioned in a manner proportional to the eigenvector coefficients of the atomic functions involved[18]. Once self-consistency was achieved for a complex ion in the manner described above, the basis set was improved by obtaining self-

-consistent atomic orbitals for the configuration obtained from the molecular calculation, and the new basis was used for converging again the molecular functions.

We have developed special integration procedures, both to improve the solution of the Schrödinger equation near each nucleus and in evaluation of $\langle\psi_i|Y_2^m/r^3|\psi_i\rangle$[19] in order to assure good precision in the calculated field gradients. The sample points used for the variational calculations for these linear molecules were obtained by considering the molecular axis as the z axis in a cylindrical coordinate system (see Fig. 1). In this manner one immediately integrates over azimuthal angle ϕ and is left with two-dimensional numerical integrations.

The x and z grids (the latter centered on each atomic site) follow a polynomial distribution $t^{2\lambda}$, where λ was adjusted to the most convenient value by trial and error. In each box of the mesh, a simple mid-point integration rule was used. For the calculations reported here, a total of 29,000 sample points was included, approximately an order of magnitude more points than were needed to obtain accurate energy eigenvalues. The main advantage of this procedure over the statistical Diophantine[13] method is that the generation of symmetrical point grids around each atomic nucleus leads to polarized charge distributions with rigorously correct symmetry, which is helpful when calculating field gradients. Thus the mutual cancellation of σ and π contributions of core levels may be accurately determined. Another advantageous feature of this symmetry-adapted grid is the possibility of reducing the computational time by integrating in only half the z-x plane for molecules with a center of inversion. Even with these precautions we found a slow convergence of core level eigenvectors with increasing number of points, toward the required 6-7 digits of precision for accurate calculation of core contributions to both δ and Δ. The simple mid-point integration rule needs to be improved to achieve a more efficient use of the integration points.

II.b Calculation of the EFG Matrix Elements

For the calculation of the quadrupole matrix elements in Eqn. 4, one-center terms were evaluated exactly, using calculated MO coefficients and the corresponding $\langle R_{nl}|r^{-3}|R_{n'l'}\rangle$ atomic radial matrix elements. The remaining two- and three-center contributions were evaluated by numerical integration[19]. The integration was carried out in spherical coordinates about the resonant gold nucleus from a radius of 0.01 a.u. to a radius of 1 a.u. using a logarithmic radial mesh and a polynomial angular mesh. The molecular volume beyond 1 a.u. was integrated using the statistical Diophantine method[13]. Matrix element precision of 3-4 significant figures was obtained with a reasonably small number of points ($\sim$ 2500).

III RESULTS AND DISCUSSION

III.a One-electron Spectra and Bonding

The energies of the molecular orbitals as well as their population analysis provide a picture of the electronic structure of the complex. The populations give information regarding chemical bonding, and the energy levels may be used to obtain electronic transition energies; these may be compared to experimental results, providing a test for the theoretical model used.

In Table I are given the energies of the occupied and of the first few unoccupied orbitals for the ground state of $[Au(CN)_2]^{-1}$, as well as their approximate composition. The interatomic distances were taken from the x-ray crystallographic study reported by Rosenweig and Cromer[20] (Au-C distance = 2.12 $\mathring{A}$, C-N distance = 1.17 $\mathring{A}$) and complete linearity of the molecule was assumed. This self-consistent result for the isolated complex

will serve as a reference point, as we study the differences between covalent and ionic bonding and the influence of the external crystalline environment.

In Fig. 2 are given energy level diagrams for $[Au(CN)_2]^{-1}$ and for the complexes $[AuCl_2]^{-1}$ and $[AuF_2]^{-1}$. The Au-Cl interatomic distance of 2.281 Å was obtained from an x-ray crystallographic study of the mixed valence compound $Cs_2Au(I)Au(III)Cl_6$ [21]. We discuss the Mössbauer data in a following section; here we wish to observe main differences in covalent versus ionic bonding of the $[AuX_2]^{-1}$ complexes. The linear complex $[AuF_2]^{-1}$ is not known to exist, but we have nevertheless performed calculations for this ion since it would be an extreme case of ionic linear bonding for Au(I). Since both covalent and ionic radii for F are smaller than for Cl, the Au-F distance considered (2.12 Å) was smaller than for Au-Cl. However, calculations performed for an expanded Au-F distance equal to 2.28 Å show no significant differences.

As can be seen from the figure, the cyanide complex has $13\sigma_g^+$ as the last occupied level, with the unoccupied $7\pi_u$ level separated by about 5eV. These levels are dominated by Au 5d,6s and 6p character respectively (see Table I). Both halide complexes have a π_g last occupied level and a gap of ∿4eV followed by an empty σ_g. Differences in the valence band width (the fluoride is narrower) and position of the halogen valence-s (low lying σ_u, σ_g pair) are consistent with the consistuent atomic levels and the greater ionicity of the fluoride. The energy levels and atomic orbital character of $[Au\ Cl_2]^{-1}$ and $[AuF_2]^{-1}$ are presented in Tables II and III respectively. We can see here that the last occupied level is dominated by halide-p character, with ∿30% Au 5d admixture. The empty σ_g level is a gold s,p,d hybrid as in the cyanide complex. The increasing ionic character $(CN)_2 < Cl_2 < F_2$ and the essentially constant filling of the Au 5d level are seen from the Mulliken atomic orbital populations and charges given in Table IV.

Now we turn to comparison with optical spectra of $[Au(CN_2)]^{-1}$ reported by Mason [22]. In Table V the experimental transitions

are compared to the calculated energy differences between the one-electron levels. In $D_{\infty h}$ symmetry, dipole transitions from the closed shell $^1\Sigma_g^+$ ground state are only allowed to $^1\Sigma_u^+$ or $^1\Pi_u$ states. The calculated values do fall in the range of the values observed; fortuitously, the $13\sigma_g^+ \rightarrow 7\pi_u$ lowest lying transition energy is in excellent agreement with experiment. In $D_{\infty h}$ symmetry, d orbitals transform according to $\sigma_g^+(d_{z^2})$, $\pi_g(d_{xz},d_{yz})$ and $\delta_g(d_{x^2-y^2},d_{xy})$ representations. Mason suggests that the total splitting of the antibonding d-levels is likely lower than 5000-7000 cm^{-1}. We find a difference in energy of 16200 cm^{-1} between the non-bonding $3\delta_g$ orbital and the last occupied $13\sigma_g^+$. This is indeed small compared to the ligand field splitting derived for tetracyanometalate complexes of D_{4h} symmetry (for example, > 50000 cm^{-1} in $[Pt(CN)_4]^{-2}$) and has been interpreted as a weaker participation of d orbitals in σ bonding in the linear case[22]. In fact, if σ bonding were stronger, the energy of the antibonding $13\sigma_g^+$ orbital would be shifted upwards. However, it must be noted that this simple ligand field picture loses much of its meaning in the present framework. As can be seen in Table I, the valence σ_g^+ orbitals show considerable mixing between Au(5d) orbitals and the ligand functions, which shows that the former do participate in bonding. However, the $13\sigma_g^+$ orbital presents a strong 6s-5d hybridization. This hybridization tends to lower the energy of the σ_g^+ level; this effect would not appear in a crystal field model.

The assignment of optical transitions as a metal→ligand charge transfer by Mason using simple qualitative ligand field arguments, is not corroborated in this calculation, since the lower energy empty orbitals are all mainly of metal character. Transitions are shown here to be between orbitals mainly localized on Au (from $13\sigma_g^+$) or as ligand→metal charge transfers.

In closing this section, we note that no rigorous agreement between experiment and theory at this level is expected, for the following reasons:

a) In the local density one-electron scheme configuration-average energies are calculated, so multiplet structure is suppressed.

b) Spin-orbit coupling, which can lead to singlet→triplet transitions with considerable intensity in Au complexes, has been completely neglected (but see below).
c) Excitation energies have been estimated from the ground state level structure; final state relaxation effects have been ignored.

Nevertheless, if past experience is any guide, the main features of the spectra and bonding for these *isolated* complexes is approximately correct.

III.b Mössbauer Isomer Shift and Quadrupole Splitting for $[AuX_2]^{-1}$ Complexes.

The use of Mössbauer spectroscopy to probe Au hyperfine fields provides a picture of the local gold chemical environment which is distinct from and complementary to one-electron spectra. In Table VI we reproduce experimental isomer shifts, δ, and quadrupole splittings, Δ, for $(AsPh_4)AuCl_2$ and $KAu(CN)_2$. Data for the latter compound were taken over a pressure range 0-43Kbar. The accepted value of Q=0.59 barn[23] in Eq. 3 was employed here in calculating Δ.

For the 77.3 KeV transition of ^{197}Au, the factor A in Eq. 1 which relates the isomer shift to $\Delta\rho(0)$ is believed to be positive[24]; the numerical value is rather uncertain. In this case, the increase of δ with covalency found experimentally would represent a corresponding increase of $\rho(0)$. As seen in Tables VII-VIII this trend is reproduced for the complexes $[Au(CN)_2]^{-1}$ and $[AuF_2]^{-1}$, but $[AuCl_2]^{-1}$ gives a higher value of $\rho(0)$ than $[Au(CN)_2]^{-1}$. Uncertainties in the interatomic distances used or basis function truncation effects could be the cause of this discrepancy. Therefore, studies were performed to determine the magnitude of effects of different atomic configurations for the basis functions, values of the atomic potential well used to stabilize the outer orbitals, etc. These show differences of $\sim$ 1-2 a.u. in the values of $\rho(0)$

obtained. Furthermore, we found that small changes in Au-C bond lengths have similar effects on $\rho(0)$. A smaller Au-C distance (2.0 Å) was found for the $[Au(CN)_2]^{-1}$ linear unit in the mixed valence compound $K_5[Au_5(CN)_{10}I_2].2H_2O$ [25]. As seen in Table VIII, if this smaller distance is considered, one gets the right trend for $\rho(0)$ in all three complexes.

A small participation of the 5s orbital in the valence molecular functions contributes to increase $\rho(0)$ in $[Au(CN)_2]^{-1}$. In $[AuCl_2]^{-1}$, the outer 3s and 3p functions of Cl contribute a non-negligible amount to the valence $\rho(0)$ on Au (orbitals $11\sigma_g^+$ and $12\sigma_g^+$). The 6s contributions decrease with decreasing covalency, as expected. We have included the core contributions (1s-4s) to $\rho(0)$ in Table VII , but since our numerical accuracy is not better than $\pm$ 1 a.u. for these densities, we prefer not to interpret calculated differences. However, differences in $\rho(0)$ for such core orbitals are shown to be very small for free atoms in different oxidation states [26].

In Table IX are contributions of the different molecular orbitals to the EFG matrix element q in the AuX_2^{-1} complexes. The main contributions are from the valence one-center terms; the two- and three-center terms and the one-center core polarization values are seen to be considerably smaller. The first entry in the Table gives results for the calculation of Δ of $[Au(CN)_2]^{-1}$ at the equilibrium distance Au-C=2.12 Å. It is seen from Table VIII that a large total negative value is obtained, although the absolute value is somewhat smaller than the experimental value of -10.2mm/sec. The point-charge contribution to the EFG of the six nearest-neighbour exterior Au ions surrounding the central atom of the complex, in the x-y plane at a distance of 3.6 Å, [20] is also included in the Table. Other exterior atoms give negligible point-charge contributions. In Table VIII we also show the value of Δ obtained considering the antishielding factor $(1-\gamma)$ for the exterior Au atoms [6,11b]; however, we believe this factor to be too large since it was obtained for the free atom and thus it does not take into account electronic rearrangements in the molecule.

From the data in Tables VIII-X one may assesss the different mechanisms producing the field gradient. Although a negative sign is indeed obtained for Δ, the simple description, assigning it to a large $6p_z$ population, is not accurate. In fact, as shown in Table IV, the 6p population obtained is very small (0.11 electrons). However, the σ-bonding levels σ_u^+, which contain Au p_z orbitals in the expansion, do give a large contribution to the EFG. In the case of $9\sigma_u^+$ this derives mainly from a small admixture of the 5p core orbital (1.8%), which is gretly magnified in the EFG one-center matrix element since the atomic $\langle r^{-3} \rangle_{5p}$ value is large. This may be thought of as an orthogonalization effect of Au states relative to ligand orbitals, which produces a contraction of the σ_u^+ orbital manifested through the participation of the inner 5p function. The main contribution of the $6p_z$ orbital (7% population) is found in the $10\sigma_u^+$ orbital, which also contains a small 5p population (0.9%). This mixing of the 5p levels with the valence orbitals may be also seen as an example of "core polarization", since the $5p_\sigma$ orbitals participate more in the valence levels than the $5p_\pi$. The $p_{x(y)}$ orbitals which form π bonds are contained in the molecular functions of π_u symmetry. The contribution to the EFG is of opposite sign, and is quite small ($6\pi_u$).

As we have mentioned, both the isomer shift δ and the absolute values of the quadrupole splittings are expected to increase with covalency. This trend is obtained with the theoretical calculations for $|\Delta|$. An analysis of the data in the Tables presented show smaller contributions of the σ_u^+ orbitals to Δ for the ionic systems; this is due mainly to smaller $6p_z$ populations with respect to $[Au(CN)_2]^{-1}$. In the case of $[AuF_2]^{-1}$, the "contraction" of the valence σ_u^+ orbitals is also significantly smaller.

From the total population obtained for the Au 5d orbital (9.7 electrons) it is seen that delocalization of these electrons to the ligands may be considered negligible. In Table X we report 5d populations found distributed over σ, π and δ symmetries, and their contributions to Δ. From this data it is seen that no back-donation occurs (the $5d(\pi)$ orbitals are not depleted), so this

mechanism can have no effect on the field gradient[8]. Only the σ electrons show a small delocalization to the ligands (σ-donation). The overall contribution of the 5d-containing orbitals is of sign opposite to the total value of Δ. Of these orbitals the $13\sigma_g^+$ presents considerable s-d hybridization with s-d cross terms contributing importantly to the matrix element q.

The inner shell one-center terms describe the core polarization, which is usually taken into account by the Sternheimer factor (1-R)[11a], based upon free ion calculations. We have attempted to evaluate core contributions directly, as part of the self-consistent calculation. We find that the total core contribution to q (orbitals up to $5\pi_u$) represents an enhancement to the valence contribution. In this sense it would correspond to a Sternheimer factor (1-R) of ∿ + 1.15.

The two and three-center contributions are largely cancelled by the nuclear terms corresponding to the C and N atoms, since the matrix elements calculated with the core functions of these atoms give values corresponding to a negative point charge at the interatomic distances considered.

III.c Role of Crystal Environment in Determining δ and Δ.

One of our goals is to understand the pressure-dependent data for $KAu(CN)_2$ shown in Table VI: a small increase in δ and an equally small *decrease* in |Δ| with increasing pressure. We have tried to reproduce this effect theoretically by performing calculations for smaller Au-C interatomic distances, keeping the C-N distance constant. The results given in Table VIII show an increase in *both* ρ(0) and |Δ| with decreasing distances. This is due to increasing Au 6s and 6p populations and greater "contractions" of valence σ orbitals for smaller metal-ligand distances.

From this data, it is clear that bonding effects in the complex ion by themselves cannot explain the experimental trend

observed for $|\Delta|$. Exterior atoms must play an important role. We have tried to include the effects of the outer atoms by means of two simple models:

a) Making self-consistent calculations for the complex in the potential field of six Au ions surrounding the central Au, with configurations that vary in the same manner as the latter, and obeying the anisotropic effect of compression observed for AuCN[9] (more effective in reducing the Au-Au distances)(*).

b) By making self-consistent calculations for the complex ion in the field of 12 K ions lying in planes above and below the $[Au(CN)_2]^{-1}$ linear unit[20], with total charge amounting to +1.

The results obtained are summarized in Table XI and Fig.3. It is seen in the Table that the inclusion of the Au exterior potentials still produces an increase in $|\Delta|$ with decreasing interatomic distances. As for the K ions, the effect obtained is to polarize charge towards the N atoms: for the calculation at the compressed distances considered (Au - C = 1.95 Å, Au - K = 4.85 Å), the value of $\rho(0)$ is decreased slightly by depletion of the 6s orbital. However, the value of Δ is almost unchanged.

III.d Relativistic Calculation for $[Au(CN)_2]^{-1}$

Since Au is an element of high atomic number, relativistic effects on the electronic structure of its compounds are expected to be important. We present here results for the energy levels of isolated atoms and $[Au(CN)_2]^{-1}$ calculated by the Dirac-Slater method[27,28] (Fig. 4) for comparison with non-relativistic results. Spin-orbit Splitting and indirect relativistic screening effects are expected to be important for gold complexes; however, the occurrence of a filled 5d shell tends to suppress some of these effects. Two main features of the relativistic atom - stabilization

---

(*) No such data are available for $KAu(CN)_2$.

of the 6s level by ∿1.6 eV, and a spin-orbit splitting of ∿1.5 eV in the 5d shell, are nearly obscured in the large number of valence MOs for the cluster. The distribution of intensity in photo-electron cross-section for the two models should be rather different; on the other hand the position and width of the valence band is similar in both cases.

The self-consistent relativistic populations obtained for Au are $5d_{3/2}(3.88)$ $5d_{5/2}(5.72)$ $6s_{1/2}(1.12)$ $6p_{1/2}(0.11)$ $6p_{3/2}$ (0.08) - higher levels: negligible. The 6s population is increased with respect to the non-relativistic case. Another feature noticed is the smaller 5p participation in the outer orbitals as was seen by the 5p total populations. This is likely caused by the lowering in energy of the $5p_{1/2}$ atomic orbital, which participates in σ bonding.

IV CONCLUSIONS

In this section we shall summarize the results obtained in this work and make a brief assessement of the successes and limitations of the model used.

We have calculated the electronic structure of $[Au\,X_2]^{-1}$ complexes for X=CN, Cl and F in an all-electron self-consistent local density scheme using a basis set of numerical atomic orbitals. Reasonably good agreement is found with optical spectra of $[Au(CN)_2]^{-1}$ and expected covalent → ionic trends are confirmed and made quantitative. Some noticible qualitative characteristics of the electronic structure of $[Au\,X_2]^{-1}$ are as follows:

a) The participation of an inner p orbital in the valence molecular orbitals of π_u symmetry. This "contraction" effect contributes considerably to the large negative values of Δ measured. Au(5d) back-donation is negligible.

b) Au (5d-6s) hybridization of the last occupied MO of σ_g^+ symmetry also contributes to enhance Δ. This effect is also

important in explaining the small crystal field splitting of the d-levels obtained in the optical spectrum of $[Au(CN)_2]^{-1}$. These features do not appear in an investigation of the electronic structure and interpretation of the hyperfine interactions using atomic models or semi-empirical valence-electrons molecular orbital calculations.

Quantitative calculations of Δ and $\rho(0)$ in the present model, may be considered reliable for the valence and outer core orbitals of Au (5s and 5p); however, the numbers obtained for $\rho(0)$ and Δ which depend on the inner core wave functions must be viewed with certain caution. For Δ, small errors in the eigenvectors introduced by the numerical integrations inherent to the method are magnified by the very large $\langle r^{-3} \rangle$ atomic core integrals. Comparing $\rho(0)$ for different compounds, as far as core terms are considered, involves very small differences between very large numbers. However, these differences were found to be quite small for free atoms in different oxidation states[26]. In this case, neglecting the inner core values of $\rho(0)$ should not affect our results significantly.

The experimental trend observed for Δ and δ going from covalent to ionic compounds is reproduced by the calculations. However, the same is not true for the variation with pressure observed for Δ in $K[Au(CN)_2]$. In this latter case, a possible cause could be the influence of Au-Au bonding, since the crystalline structure of this compound shows a layer of Au atoms[20]. The Au-Au bond is much more sensitive to compression then the Au-CN bond[9], and could have a decisive role in explaining the experimental trend. In this case, a larger cluster would be necessary for the variational calculation, or actually a band structure calculation.

We have reported preliminary results of a Dirac-Slater calculation of $[Au(CN)_2]^{-1}$, namely energy levels. However, a proper relativistic treatment of the EFG for molecular systems has not yet been worked out. Only for atomic systems the theory and applications of effective operators has been developed[29]. For molecular systems, an analogous work is now in progress.

TABLE I

level	energy (eV)	AO character
$1\sigma_g^+$	-73018.58	1s (Au)
$2\sigma_g^+$	-12184.28	2s (Au)
$1\sigma_u^+$	-11717.18	2p (Au)
$1\pi_u$	-11717.18	
$3\sigma_g^+$	-2849.21	3s (Au)
$2\sigma_u^+$	-2628.30	3p (Au)
$2\pi_u$	-2628.30	
$4\sigma_g^+$	-2214.80	3d (Au)
$1\pi_g$	-2214.80	
$1\delta_g$	-2214.80	
$5\sigma_g^+$	-597.68	4s (Au)
$3\sigma_u^+$	-502.45	4p (Au)
$3\pi_u$	-502.44	
$4\sigma_u^+$	-374.13	1s (N)
$6\sigma_g^+$	-374.13	
$7\sigma_g^+$	-327.03	4d (Au)
$2\pi_g$	-327.03	
$2\delta_g$	-327.03	
$8\sigma_g^+$	-265.03	1s (C)
$5\sigma_u^+$	-265.03	
$6\sigma_u^+$	-91.81	4f (Au)
$4\pi_u$	-91.81	
$1\delta_u$	-91.81	
$1\phi_u$	-91.81	

level	energy (eV)	AO character
$9\sigma_g^+$	-81.78	5s (Au)
$7\sigma_u^+$	-51.64	5p (Au)
$5\pi_u$	-51.48	
$10\sigma_g^+$	-18.78	2s (N), 2s (C)
$8\sigma_u^+$	-18.56	2s (C), 2s (N)
$11\sigma_g^+$	-9.19	40% 5d (Au), 2p (C), 2s (C)
$9\sigma_u^+$	-6.83	2s (C), 2p (C), 2s (N) 2% 5p (Au)
$3\pi_g$	-5.88	79% 5d (Au)
$3\delta_g$	-5.14	100% 5d (Au)
$12\sigma_g^+$	-5.07	14% 5d (Au), 2p (N), 2s (N)
$6\pi_u$	-4.33	2p (N), 2p (C)
$10\sigma_u^+$	-4.14	2p (N), 2s (N), 2p (C)
$4\pi_g$	-3.91	23% 5d (Au), 2p (N)
$13\sigma_g^+$ (a)	-3.13	40% 6s (Au), 32% 5d (Au)
$7\pi_u$	2.05	73% 6p (Au)
$14\sigma_g^+$	3.08	18% 6s (Au) 32% 7s (Au) 22% 6d (Au)
$4\delta_g$	3.98	68% 6d (Au) 32% 7d (Au)
$8\pi_u$	4.00	57% 7p (Au)

level	energy(eV)	AO character
$1\sigma_g^+$	-73015.68	1s(Au)
$2\sigma_g^+$	-12181.40	2s(Au)
$1\pi_u$	-11714.30	2p(Au)
$1\sigma_u^+$	-11714.30	
$3\sigma_g^+$	-2846.39	3s(Au)
$4\sigma_g^+$	-2722.27	1s(Cl)
$2\sigma_u^+$	-2722.27	
$2\pi_u$	-2625.47	3p(Au)
$3\sigma_u^+$	-2625.47	
$1\delta_g$	-2211.96	3d(Au)
$1\pi_g$	-2211.96	
$5\sigma_g^+$	-2211.96	
$6\sigma_g^+$	-594.93	4s(Au)
$3\pi_u$	-499.70	4p(Au)
$4\sigma_u^+$	-499.68	
$2\delta_g^+$	-324.30	4d(Au)
$2\pi_g$	-324.28	
$7\sigma_g^+$	-324.28	
$8\sigma_g^+$	-241.67	2s(Cl)
$5\sigma_u^+$	-241.67	

level	energy(eV)	AO character
$6\sigma_u^+$	-183.21	2p(Cl)
$9\sigma_g^+$	-183.21	
$3\pi_g$	-183.17	
$4\pi_u$	-183.17	
$1\phi_u$	-89.09	4f(Au)
$1\delta_u$	-89.07	
$5\pi_u$	-89.07	
$7\sigma_u^+$	-89.07	
$10\sigma_g^+$	-79.26	5s(Au)
$8\sigma_u^+$	-49.09	5p(Au)
$6\pi_u$	-49.06	
$11\sigma_g^+$	-13.62	3s(Cl)
$9\sigma_u^+$	-13.25	3s(Cl)
$12\sigma_g^+$	-4.68	42% 3p(Cl), 8% 3s(Cl) 49% 5d(Au)
$4\pi_g$	-3.79	79% 5d(Au), 21% 3p(Cl)
$3\delta_g$	-3.04	5d(Au)
$10\sigma_u^+$	-2.03	2% 5p(Au), 97% 3p(Cl)
$7\pi_u$	-1.72	3p(Cl)
$13\sigma_g^+$	-1.15	33% 6s(Au), 33% 3p(Cl) 33% 5d(Au)
$5\pi_g$ (a)	-0.67	28% 5d(Au), 72% 3p(Cl)

TABLE III

level	energy(eV)	AO character
$1\sigma_g^+$	-73015.26	1s(Au)
$2\sigma_g^+$	-12180.98	2s(Au)
$1\pi_u$	-11713.88	2p(Au)
$1\sigma_u^+$	-11713.88	
$3\sigma_g^+$	-2845.96	3s(Au)
$2\pi_u$	-2625.05	3p(Au)
$2\sigma_u^+$	-2625.05	
$1\delta_g$	-2211.53	3d(Au)
$1\pi_g$	-2211.53	
$4\sigma_g^+$	-2211.53	
$3\sigma_u^+$	-646.71	1s(F)
$5\sigma_g^+$	-646.71	
$6\sigma_g^+$	-594.48	4s(Au)
$3\pi_u$	-499.27	4p(Au)
$4\sigma_u^+$	-499.20	
$2\delta_g$	-323.87	4d(Au)
$2\pi_g$	-323.82	
$7\sigma_g^+$	-323.80	

level	energy(eV)	AO character
$1\phi_u$	-88.66	4f(Au)
$1\delta_u$	-88.62	
$4\pi_u$	-88.59	
$5\sigma_u^+$	-88.58	
$8\sigma_g^+$	-78.71	5s(Au)
$5\pi_u$	-48.59	5p(Au)
$6\sigma_u^+$	-48.29	
$9\sigma_g^+$	-19.41	2s(F)
$7\sigma_u^+$	-19.31	2s(F)
$10\sigma_g^+$	-3.65	48% 5d(Au), 48% 2p(F)
$3\pi_g$	-2.84	74% 5d(Au), 26% 2p(F)
$3\delta_g$	-2.61	5d(Au)
$8\sigma_u^+$	-1.66	2p(F)
$6\pi_u$	-1.35	2p(F)
$11\sigma_g^+$	-0.63	29% 6s(Au), 36% 5d(Au), 2p(F)
$4\pi_g$ (a)	-0.57	30% 5d(Au), 69% 2p(F)

TABLE IV

	$[Au(CN)_2]^{-1}$	$[AuCl_2]^{-1}$	$[AuF_2]^{-1}$
Au 5s	1.98	1.99	2.00
5p	5.98	6.00	6.00
5d	9.70	9.76	9.74
6s	0.64	0.611	0.531
6p	0.11	0.037	0.017
6d	0.13	0.008	0.014
7s	0.04	0.003	0.003
7p	0.04	0.006	0.004
7d	0.01	0.006	0.004
Charge	+ 0.38	+ 0.58	+ 0.69
C 2s	1.45	Cl 3s 1.99	F 2s 2.00
2p	2.86	3p 5.81	2p 5.85
Charge	- 0.31	- 0.79	- 0.84
N 2s	1.75		
2p	3.62		
Charge	- 0.38		

TABLE V

Experimental[a]		Calculated	
$\nu \times 10^{-3}$ cm^{-1}	ε (mol^{-1}cm^{-1})	$\nu \times 10^{-3}$ cm^{-1}	one-electron transition
41.74	3490	41.8	$13\sigma_g^+ \rightarrow 7\pi_u$
43.69	3740		
44.33[b]	2410		
47.39	10600	48.0	$4\pi_g \rightarrow 7\pi_u$
49.00	13200		
50.85	11000	57.4	$12\sigma_g^+ \rightarrow 7\pi_u$
51.71[b]	9280	57.6	$13\sigma_g^+ \rightarrow 8\pi_u$
54.0[c]	-	58.0	$3\delta_g \rightarrow 7\pi_u$
		58.2	$10\sigma_u^+ \rightarrow 14\sigma_g^+$
		59.7	$6\pi_u \rightarrow 14\sigma_g^+$

TABLE VI

	pressure (kbar)	δ [a] (mm/sec)	$\lvert\Delta\rvert$ (mm/sec)
$(AsPh_4)AuC\ell_2$ [b]	0	0.63	6.13
$KAu(CN)_2$ [c]	0	3.21	10.19
	27	3.45	10.08
	43	3.51	10.00

TABLE VII

Molecular Orbital $n\sigma_g^+$	$[Au(CN)_2]^{-1}$	$[Au(Cl)_2]^{-1}$	$[AuF_2]^{-1}$
1	154763.6	154763.9	154764.2
2	17121.7	17122.3	17121.1
3	3827.0	3827.0	3827.1
4	0.	0.	0.
5	950.0	0.	0.
6	0.	950.0	950.0
7	0.	0.	0.
8	0.	0.	186.13
9	186.30	0.	0.122
10	0.002	186.05	0.298
11	1.633	0.537	5.863
12	0.037	0.547	-
13	5.963	6.914	-

TABLE VIII

Complex ion	Au-C distance (Å)	Au-Au distance (Å)	$\rho(0)$ (a) (a_o^{-3})	Δ (mm/sec)					
				Electronic			nuclear contribution of atoms in complex ion (b)	nuclear contribution of 6 surrounding Au ions	Total Δ
				one center	two and three center	total			
$[Au(CN)_2]^{-1}$	2.12	3.60	387.87	-6.042	-0.843	-6.884	0.547	-0.008 (c) -0.534 (d)	-6.345 -6.871
	2.07	3.25	389.14	-6.686	-0.935	-7.621	0.586	-0.011 (c) -0.728 (d)	-7.046 -7.763
	2.01	2.93	390.53	-7.464	-1.038	-8.502	0.629	-0.015 (c) -0.996 (d)	-7.888 -8.869
	1.96	2.64	392.05	-8.397	-1.152	-9.549	0.677	-0.021 (c) -1.408 (d)	-8.893 -10.280
$[AuCl_2]^{-1}$	-	-	388.09	-4.872	-1.214	-6.086	0.948	-	-5.138
$[AuF_2]^{-1}$	-	-	384.82	-2.649	-0.774	-3.423	0.579	-	-2.844

TABLE IX

$[Au(CN)_2]^{-1}$				$[AuCl_2]^{-1}$				$[AuF_2]^{-1}$			
level	one-center (2,3-center) (a_o^{-3})	level	one-center (2,3-center) (a_o^{-3})	level	one-center (2,3-center) (a_o^{-3})	level	one-center (2,3-center) (a_o^{-3})	level	one-center (2,3-center) (a_o^{-3})	level	one-center (2,3-center) (a_o^{-3})
$1\sigma_g^+$	0.009	$8\sigma_g^+$	0. (0.062)	$1\sigma_g^+$	0.001	$1\phi_u$		$1\sigma_g^+$	0.004	$8\sigma_g^+$	-0.001
$2\sigma_g^+$	0.013	$5\sigma_u^+$		$2\sigma_g^+$	0.013	$1\delta_u$	0.003	$2\sigma_g^+$	0.012	$5\pi_u$	-0.093
$1\sigma_u^+$	0.502	$6\sigma_u^+$	0.003	$1\pi_u$	0.529	$5\pi_u$		$1\pi_u$	0.516	$6\sigma_u^+$	
$1\pi_u$		$4\pi_u$		$1\sigma_u^+$		$7\sigma_u^+$		$1\sigma_u^+$		$9\sigma_g^+$	0.018 (0.037)
$2\sigma_u^+$	0.124	$1\delta_u$		$4\sigma_g^+$	0. (0.050)	$8\sigma_u^+$	-0.343 (0.003)	$2\pi_u$	0.134	$7\sigma_u^+$	0.290 (0.029)
$2\pi_u$		$1\phi_u$		$2\sigma_u^+$		$6\pi_u$		$2\sigma_u^+$		$10\sigma_g^+$	3.142 (0.346)
$4\sigma_g^+$	0.039	$9\sigma_g^+$	0.001	$2\pi_u$	0.129	$11\sigma_g^+$	0.124 (0.075)	$1\delta_g$	0.042	$3\pi_g$	2.535 (0.010)
$1\pi_g$		$7\sigma_u^+$	-0.360 (0.003)	$3\sigma_u^+$		$9\sigma_u^+$	0.730 (0.025)	$1\pi_g$		$3\delta_g$	-7.330
$1\delta_g$		$5\pi_u$		$1\delta_g$	0.043	$12\sigma_g^+$	3.186 (0.420)	$4\sigma_g^+$		$8\sigma_u^+$	1.262 (0.029)
$3\sigma_u^+$	0.027	$10\sigma_g^+$	0.019 (0.007)	$1\pi_g$		$4\pi_g$	2.631 (0.008)	$3\sigma_u^+$	0. (0.060)	$6\pi_u$	-0.104 (0.024)
$3\pi_u$		$8\sigma_u^+$	0.001 (0.013)	$5\sigma_g^+$		$3\delta_g$	-7.327	$5\sigma_g^+$		$11\sigma_g^+$	3.134 (-0.248)
$4\sigma_u^+$	0.	$11\sigma_g^+$	1.877 (0.489)	$3\pi_u$	0.042	$10\sigma_u^+$	2.226 (0.023)	$3\pi_u$	0.068	$4\pi_g$	1.219 (0.014)
$6\sigma_g^+$	(0.016)	$9\sigma_u^+$	2.147 (0.028)	$4\sigma_u^+$		$7\pi_u$	-0.209 (0.016)	$4\sigma_u^+$			
$7\sigma_g^+$	0.007	$3\pi_g$	2.730 (0.008)	$2\delta_g$	0.010	$13\sigma_g^+$	2.989 (-0.315)	$2\delta_g$	0.016		
$2\pi_g$		$3\delta_g$	-7.460	$2\pi_g$		$5\pi_g$	1.154 (0.008)	$2\pi_g$			
$2\delta_g$		$12\sigma_g^+$	0.973 (0.036)	$7\sigma_g^+$				$7\sigma_g^+$			
		$6\pi_u$	-0.043) (0.014)	$8\sigma_g^+$	0. (0.050)			$1\phi_u$	0.004		
		$10\sigma_u^+$	1.379 (0.016)	$5\sigma_u^+$				$1\delta_u$			
		$4\pi_g$	0.925 (0.006)	$6\sigma_u^+$	0. (0.150)			$4\pi_u$			
		$13\sigma_g^+$	3.642 (-0.346)	$9\sigma_g^+$				$5\sigma_u^+$			
				$3\pi_g$							
				$4\pi_u$							

TABLE X

Orbitals	5d population	contribution to Δ (in mm/sec)	
		one-center	two and three center
$10\sigma_g^+ - 13\sigma_g^+$ (σ bonding)	1.7	-14.52	-0.42
$3\pi_g - 4\pi_g$ (π bonding)	4.0	-16.32	-0.03
$3\delta_g$ (non-bonding)	4.0	+33.30	0.0
	Total: 9.7	2.46	-0.44

TABLE XI

Au-C distance (Å)	Au-Au distance (Å)	$\rho(0)^{(a)}$ (a_o^{-3})	Δ (mm/sec)					
			Electronic			nuclear contribution of atoms in complex ion (b)	nuclear contribution of 6 surrounding Au ions (c)	Total Δ
			one-center	two and three-center	total			
2.12	3.6	385.17	-3.483	-1.265	-4.749	0.547	-0.0002	-4.202
2.07	3.25	388.10	-4.636	-1.410	-6.044	0.586	+0.0001	-5.458
1.96	2.64	395.26	-7.358	-1.664	-9.022	0.677	+0.0044	-8.341

REFERENCES

1. M.O. Faltens and D.A. Shirley, J. Chem. Phys. 53, 4249 (1970).
2. H. Prosser, F.E. Wagner, G. Wortmann and G.M. Kalvius, Hyperfine Interactions 1, 25 (1975).
3. P.G. Jones, A.G. Maddock, M.J. Mays, M.M. Muir and A.F. Williams, J. Chem. Soc. (Dalton) 1434 (1977).
4. C.A. MacAuliffe, R.V. Parish and P.D. Randall, J. Chem. Soc. (Dalton) 1426 (1977).
5. J. Danon, J. Phys., C1, 91 (1974).
6. T. Viegers, Thesis, Nijmegen University (1976) (unpublished).
7. J. Danon, "Mössbauer Effect Applications in the Coordination Chemistry of Transition Elements", IAEA, Panel Proceedings, Vienna (1972).
8. Darci M.S. Esquivel, Diana Guenzburger and J. Danon, Phys. Rev. B 19, 1357 (1979).
9. H. Prosser, G. Wortmann, K. Syassen and W.B. Holzapfel, Z. Physik, B24, 7 (1976).
10. R.R. Sharma and A.K. Sharma, Phys. Rev. Letters, 29, 122 (1972).
11. a) R.M. Sternheimer, Phys. Rev. 80, 102 (1950); 146, 140 (1966).
    b) F.D. Feiock and W.R. Johnson, Phys. Rev. 187, 39 (1969).
12. K.M. Hasselbach and W. Wurtinger, Proceedings on the Workshop in Chemical Applications of Mössbauer Spectroscopy, West Germany, 1978.
13. D.E. Ellis, Int. J. Quantum Chem. S2, 35 (1968); D.E. Ellis and G.S. Painter, Phys. Rev. B2, 2887 (1970).
14. D.A. Shirley, Rev. Mod. Phys. 36, 339 (1964).
15. J.C. Slater, "Quantum Theory of Molecules and Solids", Vol. IV, MacGraw-Hill, New York (1974).
16. W. Kohn and L.J. Sham, Phys. Rev. 140, A1133 (1965).

17. R.S. Mulliken, J. Chem. Phys. 23, 1833 (1955).

18. C. Umrigar and D.E. Ellis, Phys. Rev. (in press).

19. H.B. Jansen and D.E. Ellis, to be published.

20. A. Rosenweig and D.T. Cromer, Acta Crystallogr. 12, 709 (1959).

21. J.C.M. Tindemans - v. Eijndhoven and G.C. Verschoor, Mater. Res. Bull. 9, 1667 (1974).

22. W. Roy Mason, J. Am. Chem. Soc. 95, 3573 (1973).

23. V.S. Shirley, in "Hyperfine Structure and Nuclear Radiations", eds. E. Matthias and D.A. Shirley, North-Holland, Amsterdam (1968).

24. H.D. Bartunik and G. Kaindl, "Mössbauer Isomer Shifts in Chemical Systems of Gold", in "Mössbauer Isomer Shifts", Ed. G.K. Shenoy and F.E. Wagner, North-Holland, Amsterdam (1978), Ch. 8b.

25. C. Bertinotti and A. Bertinotti, Acta Cryst. B28, 2635 (1972).

26. J.V.Mallow, A.J. Freeman and J.P. Desclaux, Phys. Rev. B13, 1884 (1976).

27. A. Rosén and D.E. Ellis, J. Chem. Phys. 62, 3039 (1975).

28. D.A. Liberman, J.T. Waber and D.T. Cromer, Phys. Rev. 137, A27 (1965); J. Chem. Phys. 51, 664 (1969).

29. I. Lindgren and A. Rosén, Case Studies in Atomic Physics 4, 197 (1974).

TABLE CAPTIONS

Table I

One-electron energy levels (in eV) for $[Au(CN)_2]^{-1}$ complex; Au-C distance 2.12Å, C-N distance 1.17Å. Main contributions of atomic orbitals (AO) to each MO are indicated.

a) Last occupied orbital; total number of electrons is 106.

Table II

One-electron energy levels (in eV) for $[AuCl_2]^{-1}$; Au-Cl distance 2.281 Å. Main contributions of atomic orbitals are indicated.

a) Last occupied orbital; total number of electrons is 114.

Table III

One-electron energy levels (in eV) for $[AuF_2]^{-1}$; A-F distance 2.12Å. Main contributions of atomic orbitals are indicated.

a) Last occupied orbital; total number of electrons is 98.

Table IV

Populations and charges for $[AuX_2]^{-1}$[a].

a) The basis for Au was extended to include virtual levels by embedding the atom in a potential well.

b) For Au-C distance 2.12Å.

Table V

Experimental and theoretical electronic transition energies of $[Au(CN)_2]^{-1}$.

a) From Ref. (22), of $KAu(CN)_2$ in H_2O solution.

b) Shoulder.

c) Observed in solid film spectra, see Ref. (22).

Table VI

Experimental hyperfine interactions of Au(I) compounds.

(a) Relative to ^{197}Pt Pt.

(b) From Ref. (3). No measurement of the sign of Δ was made, but it may be assumed to be negative as in $[Au(CN)_2]^{-1}$.

(c) From Ref. (9).

Table VII

Values of $|\psi_i(0)|^2$ for $[AuX_2]^{-1}$ isolated complexes (in a_0^{-3}) for each molecular orbital of σ_g^+ symmetry [a].

a) Other orbitals give zero contribution.

Table VIII

Contributions to the quadrupole splitting and $\rho(0)$ for $[Au(CN)_2]^{-1}$ (at several bond lengths), $[AuCl_2]^{-1}$ and $[AuF_2]^{-1}$.

a) Orbitals 1s to 4s of Au excluded

b) $\Delta = 1.116 \sum_{i=1}^{N} Z_i \left(\frac{3z_i^2 - r_i^2}{r_i^5} \right)$ mm/sec, where N is the number of atoms in the complex ion.

c) $\Delta = 1.116 \sum_{j=1}^{M} Z_{eff} \left(\frac{3z_j^2 - r_j^2}{r_j^5} \right)$ mm/sec, where M is the number of Au atoms and Z_{eff} is their effective charge (+ 0.38 for equilibrium distance).

d) Same quantity as (c), multiplied by lattice anti-shielding factor $(1-\gamma)$ for Au (=66.58) [6,11b].

Table IX

Matrix elements $\langle \psi_i \left| \frac{3\cos^2\theta - 1}{r^3} \right| \psi_i \rangle$ where ψ_i are molecular orbitals, of $[AuX_2]^{-1}$. Two and three-center contributions, when significant, are given in parenthesis.

Table X

Contributions of Au (5d) orbitals to Δ.

Table XI

Contributions to the quadrupole splitting and $\rho(0)$ of $[Au(CN)_2]^{-1}$ at different bond lengths, in the field of 6 equatorial Au atoms.

(a) Orbitals 1s to 4s excluded.

(b) $\Delta = 1.116 \sum_{i=1}^{N} Z_i \left\{ \frac{3z_i^2 - r_i^2}{r_i^5} \right\}$ mm/sec, where N is the number of atoms in the complex ion.

(c) $\Delta = 1.116 \sum_{j=1}^{M} Z_{eff} \left\{ \frac{3z_j^2 - r_j^2}{r_j^5} \right\}$ mm/sec, where M is the number of equatorial Au atoms (6) and Z_{eff} their effective charge.

FIGURE CAPTIONS

Figure 1

Cylindrical coordinate system for linear molecules.

Figure 2

Orbital energies diagram for $[AuF_2]^{-1}$, $[AuCl_2]^{-1}$ and $[Au(CN)_2]^{-1}$.

Figure 3

Variation with interatomic distance of calculated Δ for $[Au(CN)_2]^{-1}$.

(x) Free complex ion, including contribution of 6 equatorial Au atoms as point charges.

(•) The same, with Au point charge contribution multiplied by $(1-\gamma)$

(+) Complex ion embedded in 6 Au atomic potentials.

(◈) Complex ion embedded in 12 K atomic potentials, with contribution of 6 equatorial Au atoms as point charges.

Figure 4

Orbital energies diagram for Au atom and $[Au(CN)_2]^{-1}$ for non-relativistic and relativistic calculations[(a)].

(a) Au atom configuration $5d^{10}6s^1$; atom embedded in potential well of V_o = -2a.u., radius $6a_o$ (V_o subtracted). $[Au(CN)_2]^{-1}$ calculations for Au-CN distance = 2.07 Å.

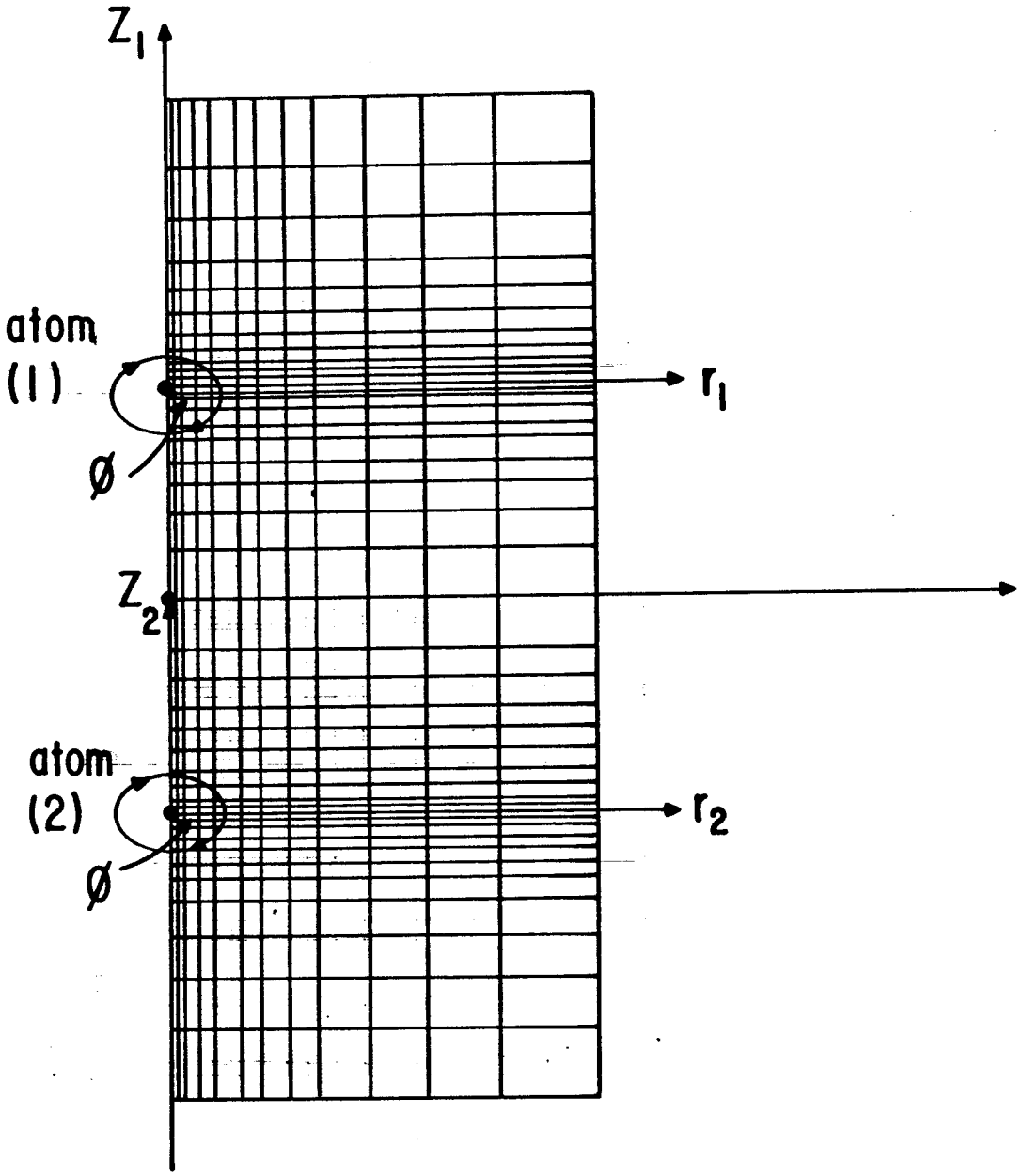

Fig. 1

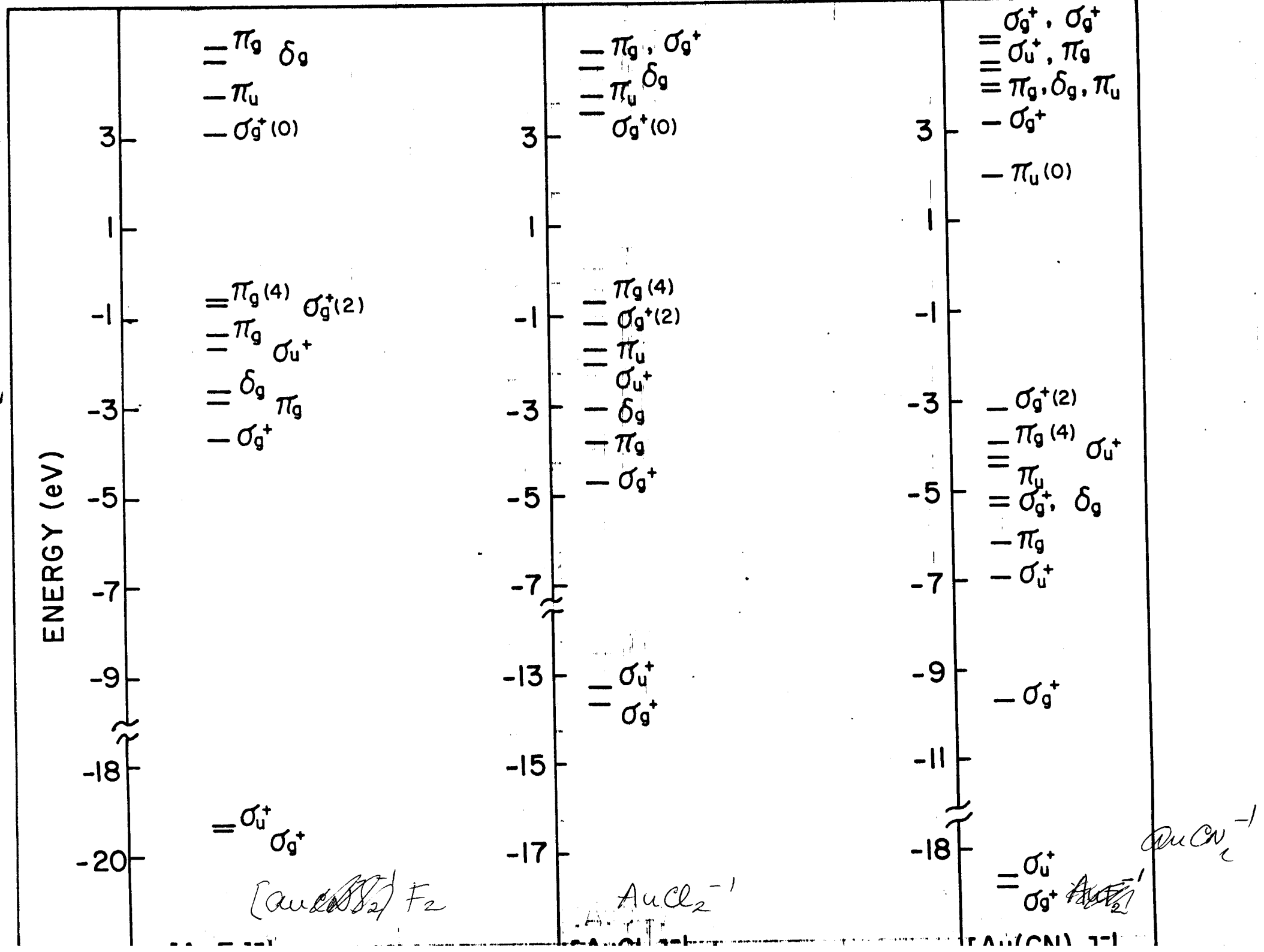
ENERGY (eV)
3
1
-1
-3
-5
-7
-9
-18
-20
π_g δ_g
π_u
$\sigma_g^+(0)$
$\pi_g(4)$ $\sigma_g^+(2)$
π_g σ_u^+
δ_g π_g
σ_g^+
σ_u^+ σ_g^+
$[AuCl_2]F_2$
π_g, σ_g^+
δ_g
π_u
$\sigma_g^+(0)$
$\pi_g(4)$
$\sigma_g^+(2)$
π_u
σ_u^+
δ_g
π_g
σ_g^+
-13
-15
-17
σ_u^+
σ_g^+
$AuCl_2^-$
σ_g^+, σ_g^+
σ_u^+, π_g
π_g, δ_g, π_u
σ_g^+
$\pi_u(0)$
$\sigma_g^+(2)$
$\pi_g(4)$ σ_u^+
π_u
σ_g^+, δ_g
π_g
σ_u^+
-11
σ_g^+
σ_u^+
σ_g^+
$AuCN_2^-$

Fig. 2

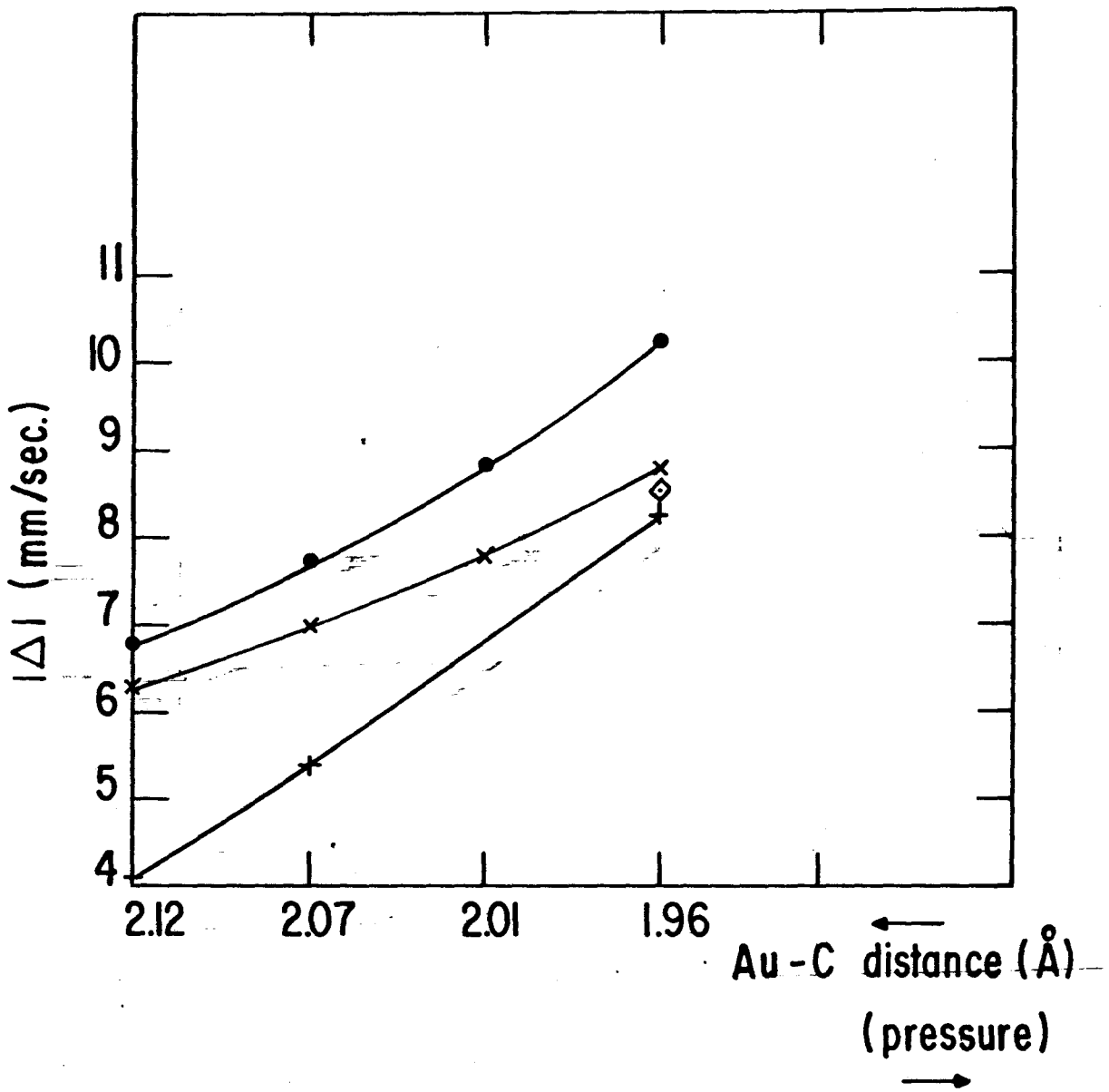

Fig. 3

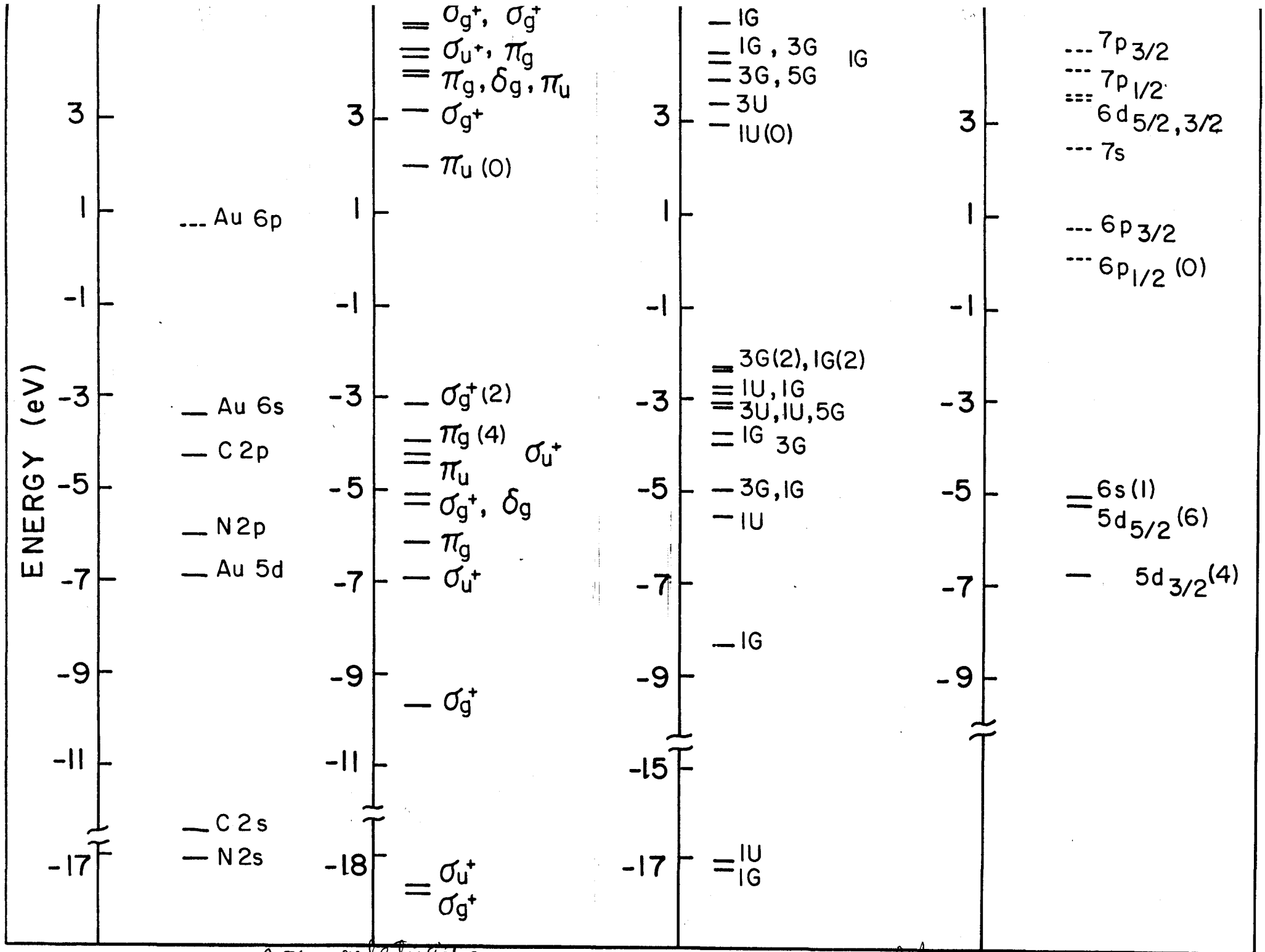
ENERGY (eV)
3
1
-1
-3
-5
-7
-9
-11
-17
Au 6p
Au 6s
C 2p
N 2p
Au 5d
C 2s
N 2s
σ_g^+, σ_g^+
σ_u^+, π_g
π_g, δ_g, π_u
σ_g^+
π_u (0)
σ_g^+(2)
π_g (4)
π_u
σ_g^+, δ_g
π_g
σ_u^+
σ_g^+
-18
σ_u^+
σ_g^+
σ_u^+
1G
1G, 3G
3G, 5G
3U
1U(0)
3G(2), 1G(2)
1U, 1G
3U, 1U, 5G
1G 3G
3G, 1G
1U
1G
-15
1U
1G
1G
7p 3/2
7p 1/2
6d 5/2, 3/2
7s
6p 3/2
6p 1/2 (0)
6s (1)
5d 5/2 (6)
5d 3/2 (4)
non - relativistic
relativistic